Journal of Biomedical Optics

BiomedicalOptics.SPIEDigitalLibrary.org

Probing differentiation in cancer cell lines by single-cell micro-Raman spectroscopy

Surekha Barkur
Aseefhali Bankapur
Madhura Pradhan
Santhosh Chidangil
Deepak Mathur
Uma Ladiwala

SPIE.

Probing differentiation in cancer cell lines by single-cell micro-Raman spectroscopy

Surekha Barkur,[a] Aseefhali Bankapur,[a] Madhura Pradhan,[b] Santhosh Chidangil,[a,*] Deepak Mathur,[c] and Uma Ladiwala[b,*]
[a]Manipal University, Department of Atomic and Molecular Physics, Manipal 576 104, India
[b]UM-DAE Centre for Excellence in Basic Sciences, Kalina Campus, Mumbai 400 098, India
[c]Tata Institute of Fundamental Research, 1 Homi Bhabha Road, Mumbai 400 005, India

Abstract. Single-cell micro-Raman spectroscopy has been applied to explore cell differentiation in single, live, and malignant cells from two tumor cell lines. The spectra of differentiated cells exhibit substantial enhancement primarily in the intensities of protein peaks with concomitant decrease in intensities of O—P—O asymmetric stretching peaks in DNA/RNA. Principal component analyses show that the spectral score of differentiated cells tends to asymptotically approach that of spectra obtained from normal neural stem cells/progenitors. This lends credence to the notion that the observed spectral changes are specific to differentiation, since upon differentiation, malignant cells become less malignant and tend toward benignity. © *The Authors. Published by SPIE under a Creative Commons Attribution 3.0 Unported License. Distribution or reproduction of this work in whole or in part requires full attribution of the original publication, including its DOI.* [DOI: 10.1117/1.JBO.20.8.085001]

Keywords: micro-Raman spectroscopy; cancer cell lines; differentiation; proteins.

Paper 150112RR received Feb. 26, 2015; accepted for publication Jun. 30, 2015; published online Aug. 5, 2015.

1 Introduction

Cancer progression is a multistep process associated with varied genetic changes that remain to be fully elucidated. Alteration in the differentiation status is one of the characteristics of cancers.[1] The differentiation status of a cancer is an important criterion for the classification of solid tumors since it is an indication of tumor aggressiveness and is, therefore, of prognostic significance.[2] We report here results of the successful application of micro-Raman spectroscopy in explorations of cell differentiation in single, live, transformed cells from two cell lines. Differentiation, as a term in biology, is generally applied to the developmental process whereby a cell—originating from the quintessential unspecialized stem cell—acquires functional specialization. Developmentally, differentiation is irreversible and, thus, unidirectional. However, in the context of cancer and according to one theory of the origin of cancer, the process can reverse and cells can dedifferentiate.[3] The extent to which dedifferentiation occurs determines the behavior of a tumor, with a highly undifferentiated tumor likely to be more aggressive and, hence, have a worse prognosis than a "well-differentiated" tumor.

Conventionally, the degree of differentiation is diagnosed histologically by comparing the structural and morphological integrity of the malignant tissue to the tissue from which it originates. Thus, a well-differentiated malignancy maintains a fair amount of organizational structure and is likely to be less invasive whereas undifferentiated tumors exhibit a near-total lack of structure with reduced cellular cohesiveness and increased invasiveness. Accordingly, both the determination of the therapeutic regimen to be followed as well as the prognosis are based on the differentiation status of the tumor.[3]

*Address all correspondence to: Santhosh Chidangil, E-mail: santhosh.cls@manipal.edu; Uma Ladiwala, E-mail: brainwave.surf@gmail.com

The mechanism of tumor differentiation is poorly understood. One of the theories, though controversial, that appears to be gaining acceptance is that cancers originate from the cancer stem cell (CSC) wherein tumors grow like normal tissues, with stem cells as progenitors of an organized system that produces new cells for tissue formation.[3] Accordingly, tumors contain a few CSCs that divide and feed tumor growth. CSCs can self-renew extensively and also produce more mature cells—called transit amplifying cells—that divide a certain number of times before differentiating into specialized tumor cells that do not divide. This model, thus, accounts for cellular heterogeneity that is commonly found in many tumors and also the propensity of CSCs to metastasize and, if not treated adequately, to produce tumor recurrence. Another model—the stochastic model of cancer growth—offers a different scenario for tumor growth. Here, it is argued that all cancer cells have the same potential to grow and divide, but each cell randomly chooses between self-renewal and differentiation. The cells in a tumor are not in an organized hierarchy—any cell has the same intrinsic potential to contribute to tumor growth.[4] It is feasible that both theories may apply, depending on the type of cancer or to different stages of tumor development.

Recently, it has been suggested that inducing differentiation might be a mode of cancer therapy that is less toxic and has fewer side effects.[5] An accurate determination of differentiation status of malignancies, thus, becomes crucial. Histopathology, after surgical removal of the specimen, remains the current mainstay of diagnosis. More sensitive, faster, and label-free methods are needed.

Vibrational spectroscopy has proved useful in understanding the biochemical changes linked to the differentiation of stem cells. Relatively few spectroscopic studies have focused on probing biochemical changes during differentiation of malignant cells. The synthesis of proteins in the early stages of stem cell differentiation has been inferred by Notingher et al. in a Raman spectroscopy study performed on differentiating embryonic stem

cells.[5,6] It was observed that the intensity of the RNA peak at 813 cm^{-1} was decreased in the Raman spectra of differentiated cells as compared to that in undifferentiated stem cells. A Fourier transform infrared spectroscopy (FT-IR) study by Ami et al. also presented the differentiation-related increase in the intensity of the amide I band in murine embryonic stem cells.[7] Raman spectroscopic markers for *in vitro* cardiogenic differentiation of human embryonic stem cells (hESCs) have been reported.[8]

Raman spectroscopy has also been used to monitor the formation of a bone-like apatite mineral during the differentiation of human mesenchymal stem cells toward an osteogenic lineage.[9] A study by Schulze et al.[9] on the differentiation status of hESCs was successful in discriminating between the Raman spectra of undifferentiated and differentiated cells by identifying intensity ratios of protein-related bands, including the 757 cm^{-1} line of tryptophan, to nucleic acid bands, including the 784 cm^{-1} line of DNA/RNA. A Raman spectroscopy study by Swain et al.[10] focused on the problem of time-dependent loss of phenotype in malignant cell lines because of spontaneous differentiation of cells in *in vitro* culture. In this study, they verified the suitability of TT1 and A549 cell lines as a model for primary human pulmonary alveolar carcinoma type I (ATII) and type II (ATII) cells, respectively, by using Raman spectroscopy as a biochemical assessment technique, and found that A549 cells are not a good model for ATII cells, whereas TT1 cells provide a reasonable model for ATI cells.

We report in the following study an exploration of single-cell micro-Raman (SCμR) spectroscopy as a possible method of quantifying the biochemical differences between specific malignant cells before and after differentiation chemically induced using all-trans retinoic acid (RA). We have used a SCμR spectrometer to explore spectral changes brought about by the differentiation in single, live, and transformed cells from two cell lines—the rat C6 glioma and human SK-N-SH neuroblastoma. Our results are encouraging in that SCμR spectroscopy does, indeed, appear to be a valid diagnostic of cell differentiation. We have also conducted micro-Raman probing of adult rat hippocampal neural progenitors/stem cells so as to make spectral comparisons of normal neural stem cells with undifferentiated and differentiated malignant cells.

2 Experimental Methods

2.1 *Cell Lines*

C6 glioma and SK-N-SH neuroblastoma cell lines used in the present experiments were cultured in Dulbecco's minimal essential medium (DMEM; Invitrogen) supplemented with 10% fetal bovine serum (FBS), 50-μg/ml penicillin and streptomycin along with 2-mM glutamine (all Invitrogen), and maintained in a CO_2 incubator at 37°C. Cells were passaged when plates were 70% to 80% confluent. For differentiation of both cell lines, RA (Invitrogen), at a concentration of 20 ng/ml, was added to differentiation medium comprising the above medium but with 2% FBS, for a period of 13 days for C6 glioma cells or 8/13 days for SK-N-SH cells.

2.2 *Isolation of Hippocampal Progenitors/Stem Cells*

Hippocampal progenitors/stem cells were isolated from Wistar rats (wt. 200 to 250 g) according to a modification of an earlier described protocol.[11] Briefly, hippocampi were dissected from brains of the rats and neural progenitor cells were isolated using a Percoll (Sigma) density gradient centrifugation. To obtain fairly pure populations of neural progenitors, the isolated cells were initially plated on poly-L-ornithine (20 μg/ml) and laminin (Invitrogen) (10 μg/ml)—coated T-25 flasks in DMEM/F-12 medium supplemented with B-27 (Invitrogen) and 40 ng/ml FGF-2 (Roche, Germany) at 37°C in a humidified atmosphere with 5% CO_2. After about 3 weeks, dense colonies of proliferating progenitor-like cells were manually stripped, mechanically dissociated, and plated in poly-L-ornithine-coated T-25 flasks (Nunc) in Neurobasal medium supplemented with B-27 and 40 ng/ml FGF-2.

2.3 *Single Cell Micro-Raman Spectroscopy*

Our micro-Raman setup, schematically shown in Fig. 1, used a diode laser (600-mW output power at 785 nm wavelength; Starbright Diode Laser, Torsana Laser Tech, Denmark) with a 2-mm beam that we expanded to 8 mm before coupling to an inverted microscope (Nikon Eclipse Ti-U, Japan). The linearly-polarized laser light was passed through a 100× oil-immersed objective (numerical aperture 1.3; Nikon, Plan Fluor) to yield a focused laser spot whose typical diameter was measured to be ~1 μm, much smaller than the diameters (typically 8 to 12 μm) of cells used in the present studies. The Raman signals were collected through the same objective by a spectrometer (Horiba Jobin Yvon *i*HR320) coupled to a liquid-nitrogen-cooled CCD detector (Symphony CCD-1024x256-OPEN-1LS) and a computer for real time recording. We used a 1200 grooves/mm grating blazed at 750 nm to permit attainment of a spectral resolution of 0.6 nm at 435 nm wavelength. However, our Raman spectrometer optics were aligned for maximum signal-to-noise ratio in measured spectra and, with the spectrometer slit width kept at 100 μm, the typical spectral resolution of our system in the course of the present series of measurements was ~5.7 cm^{-1}, as determined by measuring the full width at half maximum of the 997 cm^{-1} Raman band of a spectrum measured using polystyrene beads of 3-μm diameter. Our spectral experiments were typically performed with a constant laser power of ~25 mW. In earlier systematic studies, including those conducted on neural stem cells, we had established that power levels in excess of 50 mW increased the possibility of

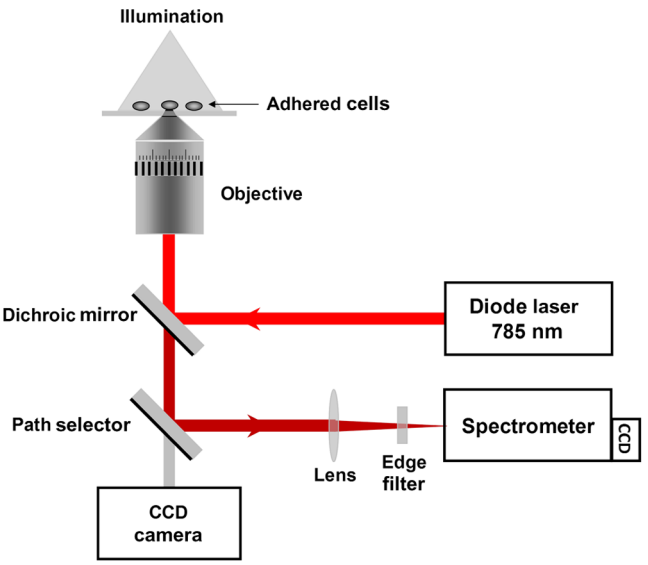

Fig. 1 Schematic diagram of our setup for single-cell micro-Raman spectroscopy.

inducing cell damage.[12–15] It is noteworthy that previous micro-Raman studies of differentiation have utilized four-fold high levels of incident power.[6,9]

As described in other reports from our laboratory,[12–15] in which the present apparatus was used in the form of a Raman Tweezers setup, we first established the absence of significant photochemistry induced by the 785-nm laser light by recording Raman spectra of a given cell for 10 min at a time, with an interval of 1 min between subsequent measurements. We ensured that all 10 spectra, thus, obtained retained the same Raman features, providing indication that no photoinduced damage was induced in the cell in the course of the experiment.

The micro-Raman measurements we performed were as follows: RA-differentiated and undifferentiated C6 glioma and SK-N-SH cells were aspirated by pipetting; they were centrifuged at 1000 rpm and washed with 1× phosphate buffered saline (PBS), and resuspended to a cell density of 5×10^5 cells/ml. Single cell suspensions were made by pipetting and vortexing cells and 20 μl of this cell suspension was loaded on a square 22 mm acid-treated, clean quartz coverslip (measured by us to be 160 ± 10 μm thick) attached to the stage of the optical trap assembly. Upon adherence of the cells to the coverslip, a single cell was randomly selected from within the microscope field of view and its spectrum measured over a time period of up to 10 min so as to obtain an adequate signal-to-noise ratio. We recorded two micro-Raman spectra from each cell, a total of 104 spectra were recorded from 52 C6 glioma cells; 80 spectra were recorded from 40 differentiated cells and 24 from 12 undifferentiated cells. Similarly, a total of 74 spectra were recorded from 37 SK-N-SH cells, 54 spectra from 27 differentiated cells, and 20 from 10 undifferentiated cells. Our micro-Raman method allows us to perform spatially-resolved spectroscopy wherein measurements can be made from selected regions of the cytoplasm and the nucleus. In the present series of measurements, we acquired spectra from both the cytoplasm and nucleus regions but did not discern any significant difference between the spectral features that we measured for differentiated and undifferentiated cells vis-à-vis the intensities of protein and DNA/RNA peaks of interest in the present study. It is noteworthy that some earlier work[16,17] has, indeed, reported that spectra measured from cytoplasm or nucleus exhibit different features. We note that spectral differences between cytoplasm and nucleus in the study of Matthäus et al.[16] was based on analysis the of C—H vibrations in the 2800 to 3000 cm^{-1} region. Our spectral region of interest is 500 to 1800 cm^{-1} and it is, therefore, not possible for us to make comparisons with features that appear in the 2800 to 3000 cm^{-1} region. The other study[17] is a confocal Raman study and, again, lack of depth information in our experiments precludes direct comparisons to be made.

It is pertinent to note here that we subjected raw spectra acquired in our experiments to 19-point moving averages smoothing and, subsequently, to baseline correction using the asymmetric least square fitting procedure proposed by Eilers.[18] The different data processing stages, depicted in Fig. 2, were carried out using standard software (MATLAB® 7.0, Grams/AI, PLS Plus IQ). We performed 2nd polynomial Savitzky-Golay, 19-point moving averages smoothing on the raw spectrum [Fig. 2(a)]. As is seen in Figs. 2(a) and 2(b), live cell spectra are inevitably superimposed on the tail of a broad fluorescence background. We removed this sloping background [Fig. 2(c)] and normalized the peak intensities using the vector normalization method. The vector normalization or 2-norm method divides the mean-centered spectra by the square root of the sum of the squared mean-centered intensities so as to make the sum of the squared intensity values in a spectrum equal to one.

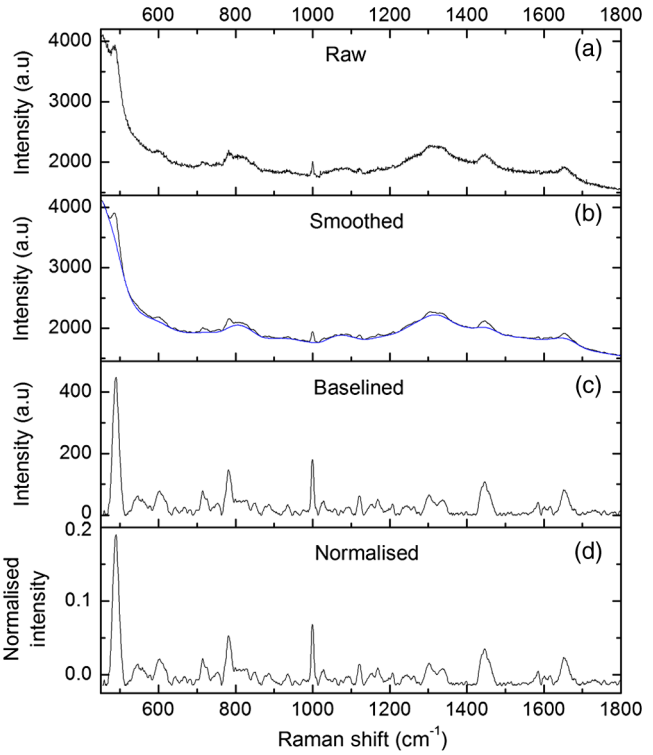

Fig. 2 Processing of raw spectral data acquired in our experiments: (a) raw spectrum of C6 cells; (b) after 19-point smoothing of the raw spectrum. The asymmetric least square baseline fit for $\lambda = 100$ and $p = 0.0001$ is shown in blue; (c) baseline-subtracted spectrum; and (d) vector-normalized spectrum of C6 cells.

2.4 *Immunofluorescence Staining for Differentiation Markers*

Both the undifferentiated and RA-differentiated C6 glioma and SK-N-SH cells were washed with 1× PBS, fixed with 4% para-formaldehyde for 15 min at room temperature (RT) and permeabilized with 0.3% Triton X-100. Blocking was by 5% horse serum in 1× PBS and cells were incubated with primary antibodies anti-glial fibrillary acidic protein (GFAP) and anti-tubulin β III for 1 h at RT. Washings were done using 1× PBS. Secondary antibodies conjugated with Alexa fluor 488 were incubated with cells for 1 h at RT. Cells were washed and counterstained with nuclear stain Hoechst for 10 min. Coverslips were mounted using gelvetol. Images were acquired on a Nikon 90i epifluorescent microscope.

3 Results and Discussion

We first present results of immunofluorescence staining that establish the differentiation status of cells used for Raman analysis. We then assign the major peaks in the Raman spectra that we measured and identify spectral features that enable differences to be probed between spectra of differentiated and undifferentiated cells.

The cytochemical evidence of differentiation induced using ATRA is presented in Fig. 3 for both cell lines used in the present studies. Figures 3(a) and 3(b) show typical bright field microscope images of undifferentiated and RA-differentiated C6

glioma cells, respectively. Undifferentiated C6 cells are seen to be morphologically different from differentiated ones: the latter have smaller, rounded cell bodies with long, slender extensions. Figures 3(c) and 3(d) are fluorescence images of GFAP expression in undifferentiated and RA-differentiated cells.

We have quantified that ~40% of differentiated cells show bright, intense GFAP expression. The remaining cells, as well as undifferentiated cells, show low levels of GFAP expression. In the case of SK-N-SH cells [Figs. 3(e)–3(h)], almost all the RA-differentiated cells, which have long processes, show

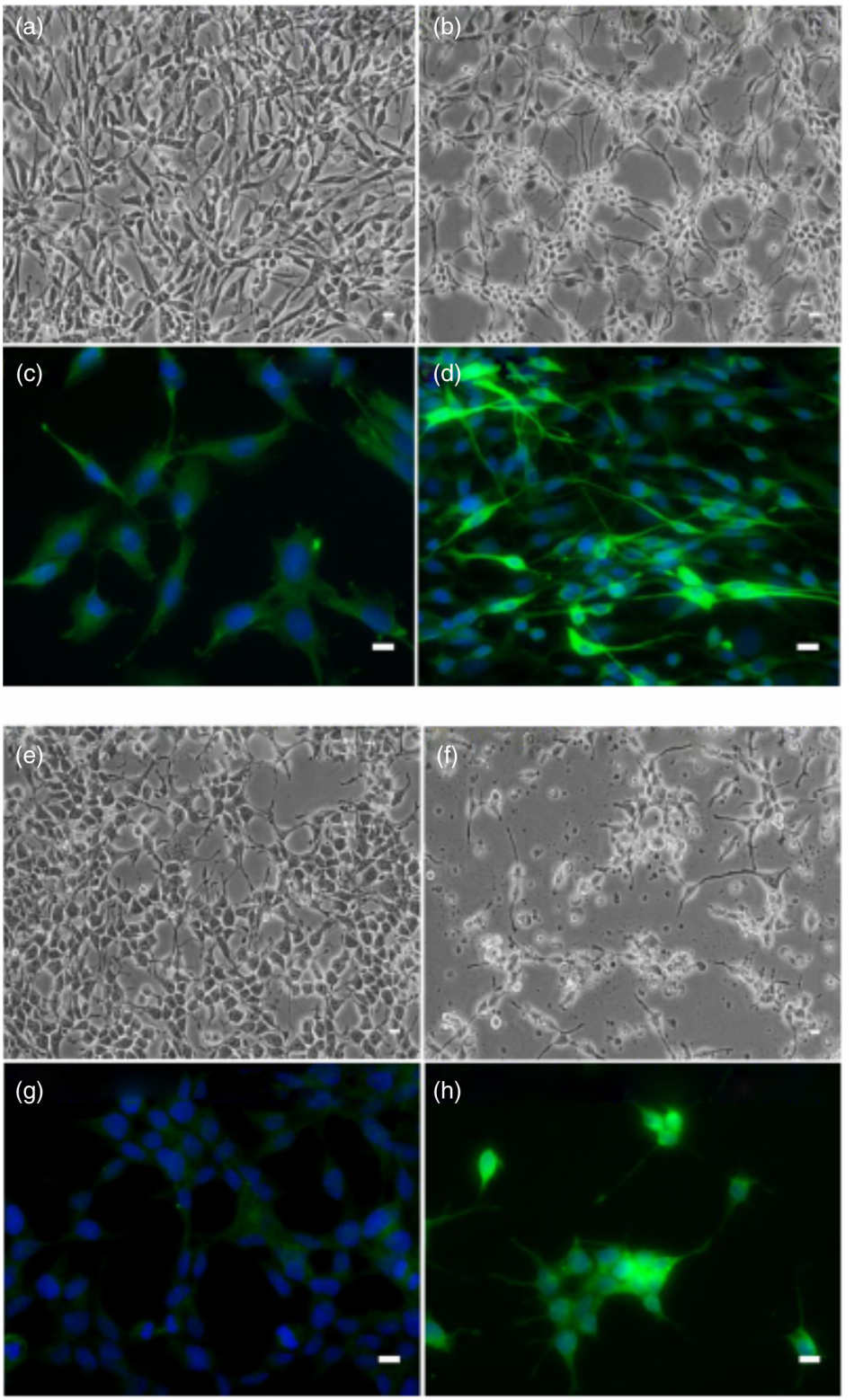

Fig. 3 Bright field microscopic images and immunofluorescence staining for differentiation markers: (a)–(d) GFAP in C6 glioma cells, and (e)–(h) beta-tubulin III in SK-N-SH neuroblastoma cells. The white scale bars in each panel denote 10 μm.

increased expression of beta-tubulin III over undifferentiated cells.

Typical micro-Raman spectra of undifferentiated and differentiated C6 glioma and SK-N-SH cells are shown in upper and lower panels of Fig. 4, respectively. The peak assignments are indicated in Table 1.

The upper panel of Fig. 4 compares the average of 24 spectra recorded from 12 undifferentiated C6 glioma cells and 80 spectra recorded from 40 differentiated C6 glioma cells, respectively. Similarly, the lower panel of Fig. 4 compares the average of 20 spectra recorded from 10 undifferentiated SK-N-SH cells and 54 spectra recorded from 27 differentiated SK-N-SH cells. As already noted, the intensity scale in each spectrum was vector-normalized, wherein the mean-centered spectra are divided by the square root of the sum of the squared mean-centered intensities so as to make the sum of the squared intensity values in a spectrum equal to one.

The Raman spectra of cells studied here are rich in contributions from proteins, nucleic acids, lipids, and carbohydrates and we have succeeded in making assignments of all major peaks. The peaks at 619, 642, 745, 848, 1000, 1029, 1175, 1206, 1606, and 1617 cm^{-1} are attributed to the various vibrations in aromatic amino acid (tyrosine, phenylalanine, and tryptophan) residues of proteins. The C—N stretching vibrations of proteins are observed at 1029, 1059, 1087 cm^{-1}, whereas the C—C stretching of protein back bone is expressed at 934 and 954 cm^{-1}. The prominent CH_2 deformation and amide I bands are visible at 1449 and 1653 cm^{-1}, respectively, whereas the amide III peak is observed at 1234 cm^{-1}. The peaks at 642 and 745 cm^{-1} can also be attributed to the C—S stretching vibrations of cysteine residues in *gauche* and *trans* conformations, respectively.

Similarly, signatures from nucleobases are observed at 642, 725, 786, 1304, 1319, 1339, 1479, and 1583 cm^{-1}. The peaks at 642 and 725 cm^{-1} correspond to the purine ring breathing mode in guanine and adenine, respectively, whereas the peak at 786 cm^{-1} has the pyrimidine ring breathing frequencies of thymine, uracil, and cytosine. The O—P—O-asymmetric stretching in DNA and RNA backbones are observed at 786 and 813 cm^{-1},

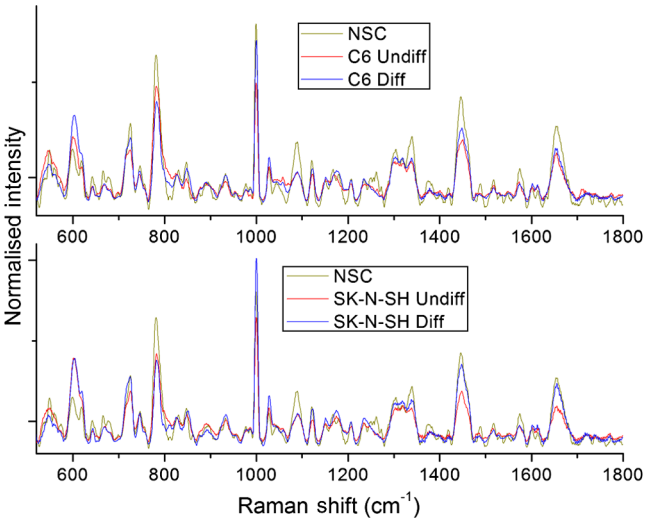

Fig. 4 Micro-Raman spectra of undifferentiated and RA-differentiated C6 glioma (upper panel) and SK-N-SH cells (lower panel) in comparison with spectra of normal neural stem cells (NSCs). The peaks in each spectrum have been vector-normalized.

Table 1 Raman frequency assignments of C6 glioma and SK-N-SH cells.

Raman frequency (cm^{-1})	Assignment	Reference
546	p: S-S str	19
562	T,G,C,A, deoxyribose	20
602	D_2 band of SiO_2	21
619	Phe: C—C twist	22
643	p: C—S str, Tyr: C—C twist, G	19·23
717	Choline: C—N sym str	23
725	A	20·24
745	p: C—S trans, Trp	20
782	DNA:O—P—O asym str, C, T,U	20·24
811	RNA:O—P—O asym str	24·25
824	Lip: O—P—O asym str	19
848	Tyr	20
934	p: bk C—C str	22·26
954	p: C—C str	22
1000	Phe: C—C skeletal	22
1028	Phe, p: C—N str	26
1059	p: C—N str, Car: C—O, DNA: C—O str	25
1087	p: C—N str	22
1122	p: C—N str, Car: C—C str	19
1151	p: C—C, C—N str, Car: C—O str	19
1175	Tyr, Phe	20·26
1207	Tyr, Phe	26
1234	p: Amide III, U	19·20
1304	A	20
1319	G	20
1339	A, G	19·27
1448	p: CH_2 def	26·28
1479	G, A	20·24
1581	G, A	24
1602	Tyr, Phe	28
1613	Tyr, Phe	22·23
1653	p: Amide I	22·23

Note: p, protein; Car, carbohydrates; Lip, lipids/phospholipids; DNA/RNA, nucleic acids; Phe, phenylalanine; Tyr, tyrosine; Trp, tryptophan; nucleobases, A,G,T,C,U; bk, backbone; def, deformation; str, stretching; asym, asymmetric.

respectively, and the peak at 1059 cm^{-1} is assigned to C—O stretching in the phosphodiester group $[(CO)_2PO_2^-]$ in the nucleic acid backbone.

Relatively few peaks from lipids/phospholipids are observed at 716 and 825 cm^{-1} corresponding to C—N stretching and O—P—O-asymmetric stretching, respectively. The carbohydrates also showed their presence through the vibrations of C—O and C—C bonds at 1059, 1151, and 1122 cm^{-1}, respectively. The observed vibrational frequencies and respective assignments are summarized in Table 1; these assignments are based on previously reported values of vibrational frequencies in biological molecules.[29–40]

Figure 5 shows the difference in marker peak intensities for undifferentiated and differentiated cells with standard deviation to indicate the data spread in our experiments. It is clear from Figs. 4 and 5 that the intensities of protein Raman peaks have increased with a concomitant decrease in intensities of O—P—O asymmetric stretching peaks from DNA/RNA in differentiated cells as compared to those in undifferentiated ones. As already noted, these spectral features are found to be independent of whether spectra were measured from the cytoplasmic region or the nuclear region of the cells. We note two facets of our experiment that might possibly account for this. Our Raman scattering signals are directed toward a wide-open slit in our spectrometer, therefore, we have no confocal rejection of out-of-focus light. This implies that we also collect signals that are generated away from the laser focus. Furthermore, the tightly focused laser beam that we use may induce some measure of optical trapping of the nucleus of the cells inside the cytoplasm even when the cell is adhered to the surface.

On comparing the average spectra from undifferentiated and RA-differentiated cells, we found that most of the peaks obtained from proteins show an increase in intensity after RA-induced differentiation. On the other hand, peaks that originate from $O—P—O^{-1}$ stretching in DNA and RNA backbones show a decrease in intensity upon RA treatment. It has been shown that synthesis of specific proteins with reduced or altered DNA/RNA expression occurs during the course of cell differentiation.[6–41,42] There is either a reduction in DNA synthesis or expression of new genes involved in the synthesis of proteins.[43,44] The experimental manifestation of this is that spectral features associated with proteins are enhanced while those associated with DNA are reduced. Thus, we surmise that our SCμR spectroscopy technique is successful in detecting significant differences between RA-differentiated and undifferentiated malignant cells. Moreover, our SCμR method permits us to experimentally deduce that enhancement of protein peaks, with concomitant diminishing of peaks ascribable to O—P—O stretching in DNA and RNA, occurs in a spatially independent fashion: the same results are obtained whether spectra are measured from the nucleus region or the cytoplasm.

To put into proper perspective the spectral differences, we carried out a principal component analysis (PCA)[45,46] comparison of spectra from C6 glioma (Fig. 6) and SK-N-SH cells (Fig. 7). PCA decomposes a set of spectra into the most common variations (factors/principle components/eigenvectors) and produces the same number of scores for each spectrum. Each spectrum's score represents its contribution to defining the various principle components. In other words, the PCA scores represent the projection of each spectrum onto the axes defined by the principle components. These scores are then used for discrimination since they provide a quantitative description of the entire set of training spectra. We used PCA to collectively analyze spectra of control and differentiated cells in order to obtain scores of factors (PCs). Our PCA was carried out over the entire range, 520 to 1800 cm^{-1}.

In the case of C6 cell spectra, it is clear from Fig. 6 that PC1 expresses the observed changes in the 619, 854, 1000, 1028, and 1183 cm^{-1} protein peaks and of the 779 cm^{-1} peak of nucleic acid O—P—O stretching; the former peaks exhibit positive intensity changes (enhancements) while the latter one shows a negative change (reduction of intensity). PC3 expresses the observed differences in the 1000, 1452, and 1651 cm^{-1} protein peaks, the 728 and 788 cm^{-1} nucleic acid peaks, and the 716 cm^{-1} lipid peak. In the case of SK-N-SH cell spectra (Fig. 7), PC1 expresses the observed differences in the protein peaks at 621, 1001, 1029, 1448, and 1655 cm^{-1} as well as in the 773 and 795 cm^{-1} peaks from nucleic acids. PC3 expresses the variations among the 1437 and 1653 cm^{-1} protein peaks, the 727, 787, and 1577 cm^{-1} peaks of nucleic acids, and the 715 cm^{-1} lipid peak.

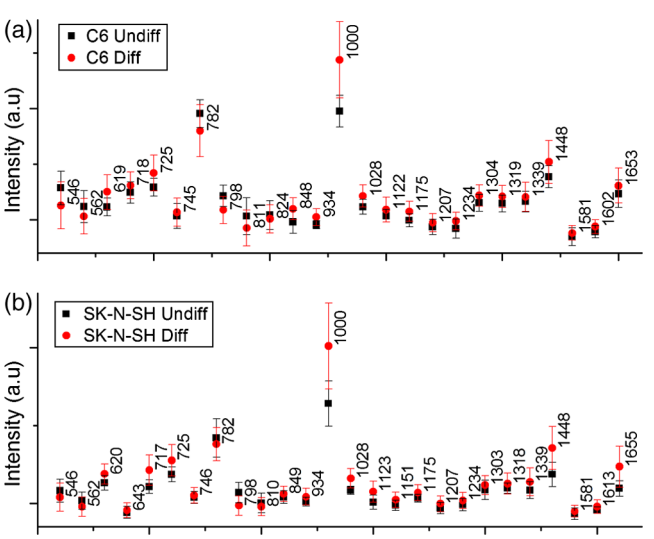

Fig. 5 Difference in marker peak intensities for differentiated (red dots) and undifferentiated (black squares) cells: (a) C6 cells and (b) SK-N-SH cells. Vertical lines denote the respective standard deviation values.

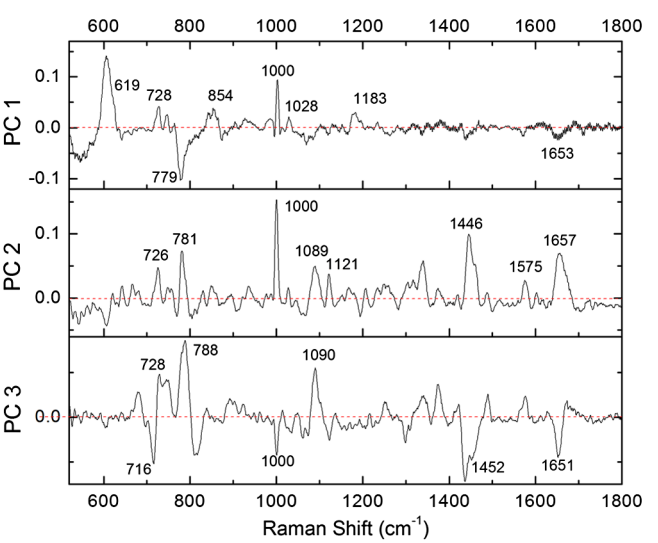

Fig. 6 Plots of PC1, PC2, and PC3 loadings (factor loading) for undifferentiated and differentiated C6 cell spectra.

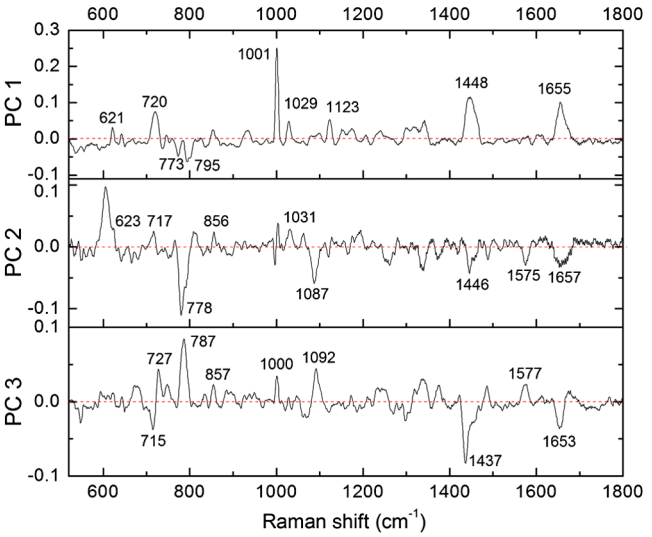

Fig. 7 Plots of PC1, PC2, and PC3 loadings (factor loading) for undifferentiated and differentiated SK-N-SH cell spectra.

A total of 114 spectral comparisons were carried out by us [10 from normal neural stem cells (NSCs), 24 from undifferentiated C6 glioma cells, and 80 from RA-differentiated C6 glioma cells] and 84 in the case of SK-N-SH cells (10 from normal NSCs, 20 from undifferentiated, and 54-from differentiated SK-N-SH cells) were loaded for PCA. In our PCA, PC1 explains 57.5% of the variance, PC2 explains 21.5% variance, and PC3 explains the next 11.5% variance in the case of C6 cells. In the case of SK-N-SH cell spectra, the PC1 explains 49% variance, PC2 explains 28% variance, and PC3 explains the next 13% variance. Consolidated results of our statistical analyses are shown in Fig. 8 in plots of the scores of PC1 and PC2.

It is evident from Fig. 8 that the spectral scores of the undifferentiated malignant cells (red dots) are clustered but those of RA-differentiated malignant cells (blue triangles) are more inhomogeneous, similar to those of normal NSCs (green squares).

There are relatively few reports in the literature on the probing of single cell differentiation by spectroscopic techniques. The advantages and difficulties of applying Raman spectroscopy to probe proliferation have been cogently summarized by Short et al.[40] whose experiments offered indications that the relative amounts of both nucleic acids and proteins increase in cells upon proliferation. In particular, exponential cells seem to possess relatively higher contents of protein, RNA, and DNA than plateau cells. In the present series of measurements, we were not able to discern substantial differences in the intensities of Raman peaks attributable to DNA. This might be indicative of the cells probed in our experiments primarily undergoing differentiation rather than proliferation. Raman experiments by Ichimura et al.[26] also offered indications that differences in the state of neuroblastoma and adipocyte cells could be visualized before and after differentiation. In the case of N2a and 3T3L1 cell lines, differentiation gave rise to increases in peak intensity attributable to cytochrome C in the cytosol and lipids.

More recently, Damayanti et al.[23] have conducted Raman studies on cell lines in different stages that are nonmalignant, premalignant, malignant, and metastatic. They observed intensity enhancements of peaks in the 1451 and 1650 cm^{-1} region of their spectra in premalignant or nonmalignant cells. These results are in conformity with our observations.

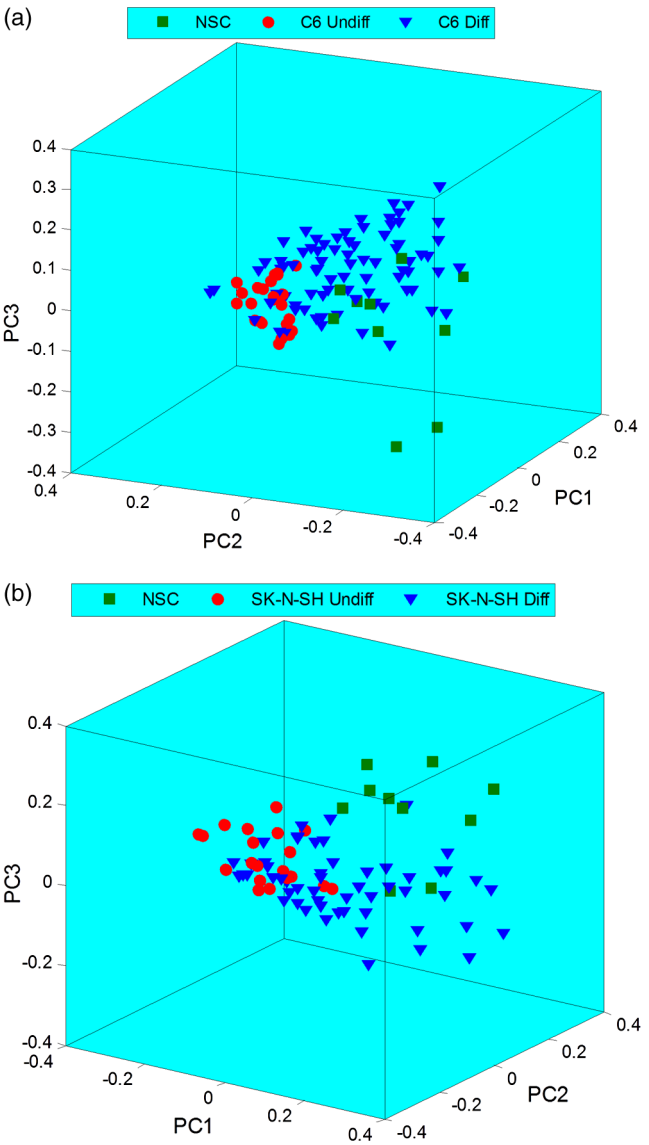

Fig. 8 Principal component analysis plots of PC1, PC2, and PC3 for NSCs (green squares), undifferentiated (red dots) and differentiated (blue triangles) cells: (a) C6 glioma cells and (b) lower panel: SK-N-SH cells.

It is noteworthy that our experiments have been conducted at incident laser power levels (25 mW) that are four-fold less than those reported in earlier measurements using 785 nm wavelength laser light.[6,9] It is pertinent to note here that the cell lines investigated in our experiments do not absorb 785-nm light, thus, precluding the possibility of direct photoinduced damage. Nevertheless, it may be possible that some nominal absorption occurs in the medium although such absorption is likely to be a more serious issue at infrared wavelengths longer than 785 nm. Direct as well as indirect thermal effects in optical traps have recently been investigated, albeit at 1064 nm wavelengths (1064 nm); we found that the rise in medium temperature that occurs within the laser focal volume amounts to only a few tens of Kelvins for values of laser power in the range 10 to 90 mW incident on hemin solution whose concentration varied over the range 0 to 50 mg/ml.[47] At power levels used in the present experiments, thermal degradation of the sample cells is unlikely to be an issue.

In summary, we have conducted micro-Raman spectroscopic investigations of single, live, malignant cells from differentiated and undifferentiated rat C6 glioma and human SK-N-SH neuroblastoma cells to probe spectral differences upon differentiation of malignant cells. Substantial enhancements in the intensities of Raman peaks associated with diverse proteins are observed in differentiated cells, with the enhanced intensities approaching those obtained with normal NSCs. The broader implications of the results we report here on two cell lines are that, in general, Raman peaks associated with lipids, polysaccharides, and amino acids might prove to be potentially useful biomarkers for monitoring the progression of tumors.

Acknowledgments

We are grateful to Dr. Yasmin Khan and Nabila Sorathia of Sophia College, Mumbai, for their assistance with C6 glioma cells. The SK-N-SH cells were acquired from the National Centre for Cell Sciences, Pune. D.M. thanks the Department of Science and Technology for the J C Bose National Fellowship. The authors thank the Department of Biotechnology for financial support for the Raman Tweezers facility under the completed project grant BT/PR6413/MED/14/802/2005.

References

1. M. Leszczyniecka et al., "Differentiation therapy of human cancer: basic science and clinical applications," *Pharmacol. Ther.* **90**, 105–156 (2001).
2. A. Jögi et al., "Cancer cell differentiation heterogeneity and aggressive behavior in solid tumors," *Upsala J. Med. Sci.* **117**, 217–224 (2012).
3. L. Vermeulen et al., "Cancer stem cells-old concepts, new insights," *Cell Death Differen.* **15**, 947–958 (2008).
4. J. E. Dick, "Looking ahead in cancer stem cell research," *Nat. Biotechnol.* **27**, 44–46 (2009).
5. I. Notingher et al., "In situ spectroscopic study of nucleic acids in differentiating embryonic stem cells," *Vibr. Spectros.* **35**, 199–203 (2004).
6. I. Notingher et al., "In situ spectral monitoring of mRNA translation in embryonic stem cells during differentiation in vitro," *Anal. Chem.* **76**, 3185–3193 (2004).
7. D. Ami et al., "Embryonic stem cell differentiation studied by FT-IR spectroscopy," *Biochim. Biophys. Acta* **1783**, 98–106 (2008).
8. L. L. McManus et al., "Raman spectroscopic monitoring of the osteogenic differentiation of human mesenchymal stem cells," *Analyst* **136**, 2471–2481 (2011).
9. H. G. Schulze et al., "Assessing differentiation status of human embryonic stem cells noninvasively using Raman microspectroscopy," *Anal. Chem.* **82**, 5020–5027 (2010).
10. R. J. Swain et al., "Assessment of cell line models of primary human cells by Raman spectral phenotyping," *Biophys. J.* **98**, 1703–1711 (2010).
11. T. Palmer, J. Ray, and F. Gage, "FGF-2-responsive neuronal progenitors reside in proliferative and quiescent regions of the adult rodent brain," *Mol. Cell. Neurosci.* **6**, 474–486 (1995).
12. A. Bankapur et al., "Probing silver nanoparticle induced stress on stem cells using Raman tweezers," *PLoS ONE* **7**, e35075 (2012).
13. E. Zachariah et al., "Probing oxidative stress in single erythrocytes with Raman Tweezers," *J. Photochem. Photobiol. B.* **100**, 113–118 (2010).
14. A. Bankapur et al., "A micro-Raman study of live, single red blood cells (RBCs) treated with $AgNO_3$ nanoparticles," *PLoS One* **9**, e103493 (2014).
15. U. Ladiwala, H. Basu, and D. Mathur, "Assembling neurospheres: dynamics of neural progenitor/stem cell aggregation probed using an optical trap," *PLoS One* **7**, e38613 (2012).
16. C. Matthäus et al., " Label-free detection of mitochondrial distribution in cells by nonresonant Raman microspectroscopy," *Biophys. J.* **93**, 668–673 (2007).
17. H. Salehi et al., "Confocal Raman data analysis enables identifying apoptosis of MCF-7 cells caused by anticancer drug paclitaxel," *J. Biomed. Opt.* **18**, 056010 (2013).
18. P. H. C. Eilers, "A perfect smoother," *Anal. Chem.* **75**, 3631–3636 (2003).
19. A. Bankapur et al., "Raman tweezers spectroscopy of live, single red and white blood cells," *PloS One* **5**, e10427 (2010).
20. J. De Gelder et al., "Reference database of Raman spectra of biological molecules," *J. Raman Spectrosc.* **38**, 1133–1147 (2007).
21. F. Liu et al., "UV irradiation-induced defect study of GeO_2-SiO_2 glasses by Raman spectroscopy," *Phys. Rev. B* **56**, 3066–3071 (1997).
22. B. Frushour and J. Koenig, "Raman spectra of D and L amino acid copolymers. Poly-DL-alanine, poly-DL-leucine, and poly-DL-lysine," *Biopolymers* **14**, 363–377 (1975).
23. N. P. Damayanti et al., "Differentiation of cancer cells in two-dimensional and three-dimensional breast cancer models by Raman spectroscopy," *J. Biomed. Opt.* **18**, 117008 (2013).
24. M. Chen et al., "Raman spectra of ten aqueous transfer RNAs and 5S RNA. Conformational comparison with yeast phenylalanine transfer RNA," *Biochemistry* **17**, 3134–3138 (1978).
25. G. J. Thomas and K. A. Hartman, "Raman studies of nucleic acids VIII estimation of RNA secondary structure from Raman scattering by phosphate-group vibrations," *Biochim. Biophys. Acta* **312**, 311–322 (1973).
26. T. Ichimura et al., "Visualizing cell state transition using Raman spectroscopy," *PLoS One* **9**, e84478 (2014).
27. G. Puppels et al., "Raman microspectroscopic approach to the study of human granulocytes," *Biophys. J.* **60**, 1046–1056 (1991).
28. Y. Zhou et al., "Human brain cancer studied by resonance Raman spectroscopy," *J. Biomed. Opt.* **17**, 116021 (2012).
29. F. S. Parker, *Applications of Infrared, Raman, and Resonance Raman Spectroscopy in Biochemistry*, Springer, Heidelberg (1983).
30. Z. Movasaghi, S. Rehman, and I. U. Rehman, "Raman spectroscopy of biological molecules," *Appl. Spectrosc.* **42**, 493–541 (2007).
31. E. Park et al., "Oxidative stress induced by cerium oxide nanoparticles in cultured BEAS-2B cells," *Toxicology* **245**, 90–100 (2008).
32. K. Erdmann, N. Grosser, and H Schröder, "L-methionine reduces oxidant stress in endothelial cells: role of heme oxygenase-1, ferritin, and nitric oxide," *AAPS J.* **7**, E195–E200 (2005).
33. W. Lin et al., "Cytotoxicity and cell membrane depolarization induced by aluminum oxide nanoparticles in human lung epithelial cells," *Toxicol. Environ. Chem.* **90**, 983–996 (2008).
34. J. Musarrat et al., "Zinc oxide nanoparticles-induced DNA damage in human lymphocytes," *Int. J. Nanopart.* **2**, 402–415 (2009).
35. C. Greulich et al., "Studies on the biocompatibility and the interaction of silver nanoparticles with human mesenchymal stem cells (hMSCs)," *Langenbeck's Arch. Surg.* **394**, 495–502 (2009).
36. B. R. Wood and D. McNaughton, "Raman excitation wavelength investigation of single red blood cells in vivo," *J. Raman Spectrosc.* **33**, 517–523 (2002).
37. B. R. Wood, B. Tait, and D. McNaughton, "Micro-Raman characterisation of the R to T state transition of haemoglobin within a single living erythrocyte," *Biochem. Biophys. Acta* **1539**, 58–70 (2002).
38. B. R. Wood et al., "Resonance Raman spectroscopy of red blood cells using near-infrared laser excitation," *Anal. Bioanal. Chem.* **387**, 1691–1703 (2007).
39. S. Hu et al., "Assignment of protoheme resonance Raman spectrum by Heme labeling in myoglobin," *J. Am. Chem. Soc.* **118**, 12638–12646 (1996).
40. K. W. Short et al., "Raman spectroscopy detects biochemical changes due to proliferation in mammalian cell cultures," *Biophys. J.* **88**, 4274–4288 (2005).
41. F. C. Pascut et al., "Non-invasive label-free monitoring the cardiac differentiation of human embryonic stem cells in-vitro by Raman spectroscopy," *Biochim. Biophys. Acta* **1830**, 3517–3524 (2013).
42. E. Zuser et al., "Confocal Raman microspectral imaging (CRMI) of murine stem cell colonies," *Analyst* **135**, 3030–3033 (2010).
43. Q. Liu et al., "All-trans retinoic acid induced the differentiation of human glioma cells," *Clin. Oncol. Cancer Res.* **8**, 42–46 (2011).
44. F. Cimmino et al., "Comparative proteomic expression profile in all-trans retinoic acid differentiated neuroblastoma cell line," *J. Proteome Res.* **6**, 2550–2564 (2007).

45. B. Wu et al., "Comparison of statistical methods for classification of ovarian cancer using mass spectrometry data," *Bioinformatics* **19**, 1636–1643 (2003).
46. S. N. Raja et al., "Serum protein profile study of normal and cervical cancer subjects by high performance liquid chromatography with laser-induced fluorescence," *J. Biomed. Opt.* **13**, 054062 (2008).
47. P. Kumari et al., "Optical trapping in an absorbing medium: from optical tweezing to thermal tweezing," *Opt. Express* **20**, 4645–4652 (2012).

Surekha Barkur received her master's in photonics at Manipal University and is currently undertaking doctoral research on Raman spectroscopy and surface-enhanced Raman spectroscopy of blood components. Her broad research interests include biophotonics, nanobiophotonics, and molecular spectroscopy.

Aseefhali Bankapur is currently an assistant professor in Manipal University's Department of Atomic and Molecular Physics, working on the design and development of Raman tweezers for biomedical applications. He regularly delivers lectures to postgraduate students in photonics and in nanoscience and technology. His other research interests are cell-nanoparticle interactions and nanoparticle-based gene delivery systems.

Madhura Pradhan received her PhD in applied biology from the University of Mumbai for her oncology-based research involving the identification and studies of novel drug targets in chronic myeloid leukemia. Her current research interests involve studies of novel drugs that alter the actin and tubulin dynamics in cancer cells and to understand the process of invasion and metastasis in brain and breast cancer.

Santhosh Chidangil received his PhD in physics from Banaras Hindu University. He heads Manipal University's Department of Atomic and Molecular Physics and his research interests include micro-Raman spectroscopy, interaction of ultrashort laser pulses with biological macromolecules, proteomics and protein profiling of body fluids, remote ultratrace analysis using LIBS, and development of fluorescence and Raman spectroscopic methods for diagnosis of various cancers.

Deepak Mathur received his PhD in physics from the University of London. After working at University College London and Birkbeck College London, he joined Tata Institute of Fundamental Research in Mumbai, where he is currently a distinguished professor, to initiate research in the atomic and molecular sciences. His current research interests include ultrafast phenomena in atoms and molecules, matter in strong optical fields, biological physics, and photonics.

Uma Ladiwala received her MD in pathology from the University of Mumbai. Her postdoctoral work in Mumbai and Sweden/Canada was in the neuroimmunology of leprosy and multiple sclerosis. She was, until recently, a member of the life sciences faculty at the UM-DAE Centre for Excellence in Basic Sciences in Mumbai. Her research interests include studies of immune and biophysical aspects of adult neural stem cells, amyloid/nanoparticle/neural cell interactions, and adhesion and differentiation of brain cancer cells.